City Research Online

City, University of London Institutional Repository

Simultaneous Measurement of Strain and Temperature with a Few-Mode Fiber-based Sensor

Chenxu Lu, Juan Su, Xiaopeng Dong, Tong Sun and Kenneth T. V. Grattan

Abstract—**This paper proposes a novel detection scheme simultaneously to measure strain and temperature, based on a simple to construct device using a section of a specially designed few mode fiber (FMF). The parameters and index profile of the FMF used as the key sensor element are such that the fiber supports only the LP_{01} and LP_{02} modes. The propagation constant difference between LP_{01} and LP_{02} modes, $\Delta\beta$, has a maximum corresponding to the critical wavelength (CWL) in the fiber transmission spectrum. Because the two peaks located closest to the CWL from both sides, Left Peak 1 and Right Peak 1, shift in opposite directions, with different sensitivities under axial strain and temperature variations, the FMF device is capable of measuring the strain and temperature simultaneously. A theoretical analysis has been carried out as part of the design process and the experimental results obtained are found to agree well with the theoretical predictions. The characteristics of this sensor scheme is discussed in light of other competing approaches to simultaneous temperature and strain monitoring and is found to show advantages which suit several practical applications including compactness, ease of fabrication and implementation, relatively high sensitivities and low cost.**

Index Terms—**Fiber optics sensor, few mode fiber, intermodal interference, critical wavelength, strain sensor, temperature sensor.**

Chenxu Lu is with the Institute of Lightwave Technology, School of Information Science and Technology, Xiamen University, Xiamen, Fujian 361005, China, and is with the School of Mathematics, Computer Science and Engineering, City, University of London, Northampton Square, London, EC1V 0HB, United Kingdom. (e-mail: Chenxu.Lu@city.ac.uk).

Juan Su is now with the Institute of Marine Science and Technology, Shandong University, Jinan, Shandong 250100, China. She was pursuing the doctoral research in the Institute of Lightwave Technology, School of Information Science and Technology, Xiamen University, Xiamen, Fujian 361005, China, during the completion of this work. (e-mail: sujuan@sdu.edu.cn).

Corresponding author Xiaopeng Dong is with the Institute of Lightwave Technology, School of Information Science and Technology, Xiamen University, Xiamen, Fujian 361005, China (e-mail: xpd@xmu.edu.cn).

Tong Sun is with the School of Mathematics, Computer Science and Engineering, City, University of London, Northampton Square, London, EC1V 0HB, United Kingdom. (e-mail: t.sun@city.ac.uk).

Kenneth T. V. Grattan is with the City Graduate School and the School of Mathematics, Computer Science and Engineering, City, University of London, Northampton Square, London, EC1V 0HB, United Kingdom. (e-mail: K.T.V.Grattan@city.ac.uk)

I. INTRODUCTION

OPTICAL fiber sensors, which can measure strain and temperature simultaneously, have potential applications in many industrial processes such as structural health monitoring, various industrial fabrication processes and in other optical fiber sensors and various designs of such sensor systems have been intensively studied over recent years. Such methods for the simultaneous measurement of strain and temperature can be categorized as follows: i) two individual sensors with different sensitivities to strain and temperature, such as two fiber Bragg grating (FBG) with different grating periods [1], different types of fiber structure [2], using emission lines [3], long period gratings [4] or fluorescent fiber techniques [5]; ii) one single sensor with two or more outputs which show different responses to strain and temperature (such as the peak or dip wavelengths formed by interference between two different orders of core/cladding modes with the fundamental mode in one compact fiber interferometer) constructed by splicing a suspended core photonic crystal fiber [6], a liquid-filled photonic crystal fiber [7], or a fiber taper and lateral-shifted junction [8] with normal single mode fiber (SMF). In some of these designs, the use of two sensors located at different positions can cause errors in the measurement of one or the other measurand (as they are not co-located). Alternatively, where the dual-sensor is placed at only one location (for both strain and temperature detection), sensors based on detection of two peak or dip wavelengths obtained from the transmission spectrum of multimode interferometer often involve a high degree of complexity in the signal analysis and/or the device fabrication and interrogation processes required, which then together may restrict their practical applications in industry. Thus alternative approaches to the sensor design are needed.

In some in-line Mach-Zehnder interferometers (MZIs) (constructed by splicing multimode fiber (MMF) or few mode fiber (FMF) between two pieces of SMF – termed SMS or SFS structures), a critical wavelength (CWL) may appear in the transmission spectra of the LP_{01}-LP_{02} mode interference [9-15]. The peaks that lie closest to the CWL at each side have their maximum spacing from the adjacent peaks and thus it is easy to identify them from the interference fringes seen. Moreover, the peaks on each side of the CWL will move in opposite directions when experiencing strain and temperature variations: also the peak temperature/strain sensitivities increase greatly as they are

close to the CWL, whether on the left or right side [14]. Previous studies by some of the authors [12-15] indicate that an exclusive value of the CWL may exist in the transmission spectrum of a SFS structure employing a specially designed FMF, which supports only two modes, LP_{01} and LP_{02} [16] and the interference between these two modes may produce a stable and polarization-independent transmission spectrum [17]. The peaks closest to the CWL on each side exhibit maximum strain/temperature sensitivities and they shift in opposite directions, with different strain/temperature sensitivities. This forms the basis of the sensor design discussed in this work.

In this paper, a novel compact in-line MZI dual-parameter sensor which can simultaneously measure strain and temperature is theoretically analyzed as the basis of an optimum design, before being experimentally fabricated and the sensor demonstrated for the first time. The core of the sensor itself can be readily fabricated by splicing a section of 20cm FMF between two segments of 'standard' SMF. Arising from the transmission spectrum of SFS structure, the two peaks closest to the CWL (at both sides) have the advantages of relatively high (and indeed different) sensitivities, ease of identification and detection, and thus it is practicable to use this SFS structure-based sensor system to allow excellent simultaneous discrimination of strain and temperature, in the sensor device that has thus been developed.
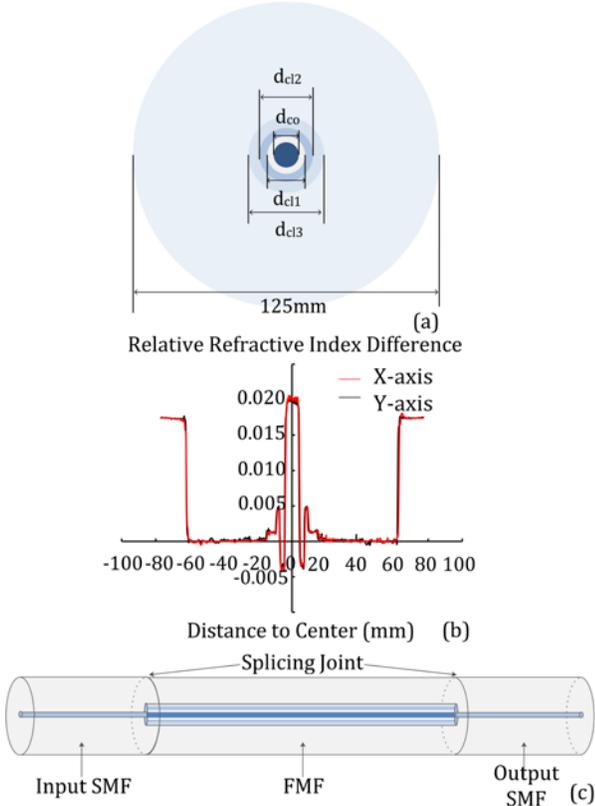
II. THEORETICAL ANALYSIS

Fig. 1. Structure of FMF and SFS. (a) Geometrical structure of FMF; (b) Relative refractive index difference profile of FMF measured at 670nm. The parameters used in the calculation are: d_{co}=8μm, $Δn_{co}$=1.99%, d_{cl1}=14.3μm, $Δn_{cl1}$=–0.40%, d_{cl2}=18μm, $Δn_{cl2}$=0.48%, d_{cl3}=30μm, $Δn_{cl3}$=0.14%. (c) Diagram of the SMF-FMF-SMF (SFS) structure.
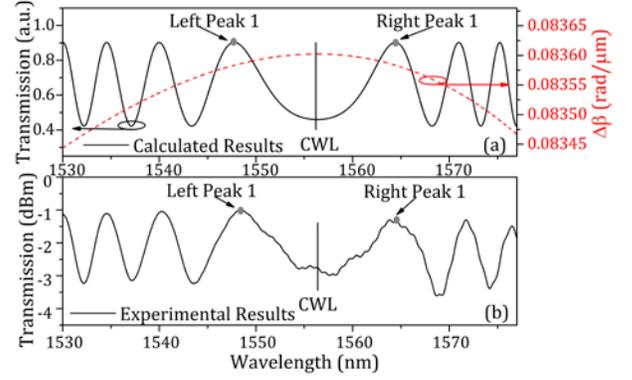

Fig. 2. Calculated $Δβ$ vs. wavelength, simulated and experimental transmission spectrum of the SFS structure with straight unstrained 20cm FMF at a temperature of 25ºC: (a) Calculated results of $Δβ$ and transmission spectrum. (b) Experimental results of transmission spectrum.

The FMF used in this work has been specially designed such that the fiber supports only the fundamental mode, LP_{01}, and the first circularly symmetric higher order core mode, LP_{02} propagating in the fiber at the operational wavelength [16]. To realize that, the FMF has a highly GeO_2-doped core region and first-third special designed inner cladding regions, as shown in Fig. 1 (a) and (b). The relative refractive index difference is defined as $Δn_{co/cli} = (n_{co/cli} - n_0)/n_0$, where $n_{co/cli}$ and n_0 are the refractive indices of core/ith inner cladding and pure silica of FMF, respectively. The inner cladding with a positive relative refractive index difference value is defined as the 'ridge', while the one with a negative value is called the 'trench'. For the FMF used in this paper, the first inner cladding is a F-doped trench immediately adjacent to the core, surrounded by a GeO_2-doped ridge with a refractive index difference such that $Δn_{cli3}<Δn_{cli2}< Δn_{co}$, in turn surrounded by another GeO_2-doped rigde and then a pure SiO_2 outer cladding region.

The SFS structure was formed by splicing a piece of FMF between two segments of SMF, as shown schematically in Fig. 1 (c). The LP_{01} and LP_{02} modes propagating in the FMF are excited by the fundmental mode LP_{01} in the input SMF. The interference between the LP_{01} and LP_{02} modes is transmitted by the output SMF. If the ratios of optical power transferred to the LP_{01} and LP_{02} modes in the FMF from the input SMF are $t_{01} = P_{01}/P_{in}$ and $t_{02} = P_{02}/P_{in}$, respectively, the transmission, T, through the SFS structure is simply given by [8]:

$$T=P_{out}/P_{in}=t_{01}^2 + t_{02}^2 + 2t_{01}t_{02}\cos(\varphi(\lambda)) \qquad (1)$$

where $\varphi(\lambda)$ is the phase difference between LP_{01} and LP_{02} modes in the FMF, which can be represented by:

$$\varphi(\lambda) = \Delta\beta \cdot L \qquad (2)$$

where L is the physical length of the FMF. $\Delta\beta=\beta_{01} - \beta_{02}$ is the propagation constant difference between LP_{01} and LP_{02} modes of the FMF. β_{01} and β_{02} are the propagation constants of the LP_{01} and LP_{02} modes in the FMF, respectively. With the parameters given in Fig. 1, using a finite element method

analysis, the simulated $\Delta\beta$ vs. wavelength at a temperature of 25^0C with zero axial strain is depicted as the dashed line in Fig. 2 (a). The calculated transmission spectrum of the SFS structure, of 20cm length FMF, combining (1) and $\Delta\beta$ is shown as a solid line in Fig. 2 (a). The corresponding experimental transmission spectrum is depicted in Fig. 2 (b), (and this agrees well with the simulated results obtained). Since the dispersion of $\Delta\beta$ exhibits a non-linear behavior (and has a turning point which corresponds to the CWL in the transmission spectrum), the periods of the interference fringe closest to the CWL from both sides reach the maximum. The peaks closest to the CWL from the left and right sides are denoted as Left Peak 1 and Right Peak 1, (and these two peak wavelengths are represented as λ_{L1} and λ_{R1}, respectively).

The wavelength shift of a given peak arising from the perturbation (strain or temperature) variations can be written as [10]：

$$\frac{\Delta\lambda}{\Delta\chi} = -\frac{1}{L}\left(\frac{\partial\varphi}{\partial\chi}\right)\left(\frac{\partial(\Delta\beta)}{\partial\lambda}\right)^{-1} \quad (3)$$

where $\partial\varphi / \partial\chi$ is the strain or temperature induced phase difference. $\partial\varphi / \partial\chi$ and L are both positive quantities at the operational wavelength, λ [10]. For peaks on the lower wavelength side of the CWL (i.e., within the region from 1500nm to the CWL), there is a blue shift because $\partial(\Delta\beta)/\partial\lambda$ is positive. However, for peaks on the longer wavelength side of the CWL (i.e., within the region from the CWL to 1580nm), there is a red shift because $\partial(\Delta\beta)/\partial\lambda$ is negative. Moreover, because $\Delta\beta$ changes non-linearly with wavelength and reaches its maximum value at the CWL, the peaks closest to the CWL show large and indeed different strain or temperature wavelength sensitivities with $\partial(\Delta\beta)/\partial\lambda \rightarrow 0$ near the CWL. However, the mathematical-derived infinitely high sensitivity at the CWL has no practical value for $\partial(\Delta\beta)/\partial\lambda$=0 at CWL. Since the Left/Right peak 1 show the highest strain and temperature sensitivities among all the peaks located at the left/right side of the CWL, these two peaks are the basis in the practical sensor device to measure both strain and temperature simultaneously.

Assuming the axial strain and temperature sensitivities of Left Peak 1 are $K_{\varepsilon L}$ and K_{TL}, respectively, then with an axial strain variation of $\Delta\varepsilon$ and a temperature variation of ΔT, the wavelength response of Left Peak 1, $\Delta\lambda_{L1}$, to axial strain and temperature can be expressed as $\Delta\lambda_{L1}=K_{\varepsilon L}\Delta\varepsilon+K_{TL}\Delta T$. For Right Peak 1 with strain and temperature sensitivities of $K_{\varepsilon R}$ and K_{TR}, respectively, the wavelength response, $\Delta\lambda_{R1}$, to axial strain and temperature can be expressed as $\Delta\lambda_{R1}=K_{\varepsilon R}\Delta\varepsilon+K_{TR}\Delta T$. Therefore, the approach proposed to measure simultaneously the strain and temperature using the SFS structure discussed can be achieved through finding the

solutions to the following sensor matrix equation [19]:

$$\begin{pmatrix} \Delta\lambda_{L1} \\ \Delta\lambda_{R1} \end{pmatrix} = \begin{pmatrix} K_{\varepsilon L} & K_{TL} \\ K_{\varepsilon R} & K_{TR} \end{pmatrix}\begin{pmatrix} \Delta\varepsilon \\ \Delta T \end{pmatrix} \quad (4)$$

The change of axial strain and temperature can be simultaneously determined by solving (4):

$$\begin{pmatrix} \Delta\varepsilon \\ \Delta T \end{pmatrix} = \frac{1}{D}\begin{pmatrix} K_{TR} & -K_{TL} \\ -K_{\varepsilon R} & K_{\varepsilon L} \end{pmatrix}\begin{pmatrix} \Delta\lambda_{L1} \\ \Delta\lambda_{R1} \end{pmatrix} \quad (5)$$

where $D = |K_{\varepsilon L}K_{TR} - K_{TL}K_{\varepsilon R}|$ is the absolute value of the determinant of the coefficient matrix. According to the error analysis method given in [20], if an optical spectrum analyzer (OSA) has wavelength measurement resolution of $\delta(\Delta\lambda_{L1})$ and $\delta(\Delta\lambda_{R1})$ at these wavelengths, the theoretical strain and temperature resolutions of the sensor scheme discussed, $\delta(\Delta\varepsilon)$ and $\delta(\Delta T)$ can be represented by:

$$\begin{pmatrix} \delta(\Delta\varepsilon) \\ \delta(\Delta T) \end{pmatrix} = \pm\frac{1}{D}\begin{pmatrix} |K_{TR}| & |K_{TL}| \\ |K_{\varepsilon R}| & |K_{\varepsilon L}| \end{pmatrix}\begin{pmatrix} \delta(\Delta\lambda_{L1}) \\ \delta(\Delta\lambda_{R1}) \end{pmatrix} \quad (6)$$

III. EXPERIMENTAL CONFIGURATION

The schematic diagram of the experimental setup of the sensor scheme that was designed and used is shown in Fig. 3. To create this practical sensor device, a piece of FMF was spliced between two sections of standard SMF (Coring SMF-28e) to form the SFS (SMF-FMF-SMF) structure. The fusion splicing was performed with an automatic fusion splicer (Ruiyan, RY-F600P), where the length of the FMF is 20cm. To investigate the response of the SFS structure to axial strain, the input SMF was fixed on a stage and the output SMF was spliced to a FBG, which has an axial strain sensitivity of 1.2pm/με. One side of a spring was fixed to a translation stage and the other side was fixed to the pigtail of the FBG and thus the same axial strain was applied to both the FMF and FBG simultaneously when the translation stage moves. The FMF section is also heated in an electrically-controlled temperature oven and the sensor transmission spectra were measured in-line using an Er-doped ASE broadband light source and an Optical Spectrum Analyzer (OSA).
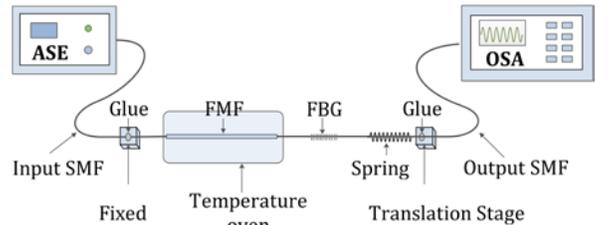

Fig. 3. Experimental setup of the strain and temperature sensor based on the SFS structure. ASE – amplified spontaneous emission source; OSA – Optical Spectrum Analyzer; SMF – single mode fiber; FMF – few mode fiber; FBG – Fiber Bragg Grating.

The sensing response of the SFS structure to strain and temperature was measured, separately for each parameter. The strain coefficients were measured at room temperature (noted

to be 25.3°C). Figure 4 shows the measured transmission spectra of the SFS structure under different levels of axial strain. It is obvious that Left Peak 1 shifts to the blue and Right Peak 1 shifts to the red as the axial strain increases, which is consistent with the theoretical analysis. The wavelength shifts of Left Peak 1 and Right Peak 1 are shown in Fig. 5. Within the axial strain range from 0 to 600με, both Left Peak 1 and Right Peak 1 shift linearly, with strain sensitivities of -0.013nm/με and 0.009nm/με, respectively.

The temperature sensitivities of Left Peak 1 and Right Peak 1 were measured by heating the oven over the range from 25.3°C to 58°C. The transmission spectra and wavelength responses of Left Peak 1 and Right Peak 1 are shown in Fig. 6 and Fig. 7, respectively. Similar to the strain characteristics observed, over the temperature range from 25.3°C to 58°C, the Left Peak 1 exhibits a blue shift with a temperature sensitivity of -0.212nm/°C, while the Right Peak 1 exhibits red shift with a temperature sensitivity of 0.262nm/°C. Linear regression analysis gives correlation coefficients of ≥0.990 for all four relationships within a strain range of 0-600με over the temperature range studied, from 25.3 to 58°C.

As shown in Fig. 4 and Fig. 6, the transmission spectra of the SFS sensor change periodically when the applied axial strain or temperature increases. The peaks used for measurement may show problems due to spectral overlap when the applied axial strain or the temperature goes beyond the accessible measurement range. Therefore, the strain and temperature measurement range of the SFS sensor, as reported, is limited to 0-600με and 25-58°C, respectively. Extending this sensor range is the subject of further study, as the more limited dynamic range seen is a drawback in a practical instrument.
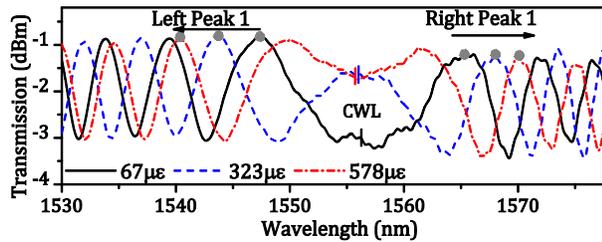

Fig. 4. Transmission spectra of the SFS sensor under axial strains of 67με, 323με and 578με.

Because the strain and temperature coefficients of the sensor matrix (4) are $K_{\varepsilon L}$ = -0.013nm/με, $K_{\varepsilon R}$ =0.009nm/με, K_{TL} = -0.212nm/°C, and K_{TR} = 0.262nm/°C, the values of $\Delta\varepsilon$ and ΔT can be calculated by using the following matrix:

$$\begin{pmatrix} \Delta\varepsilon \\ \Delta T \end{pmatrix} = \frac{1}{0.0015} \begin{pmatrix} 0.262 & 0.212 \\ -0.009 & -0.013 \end{pmatrix} \begin{pmatrix} \Delta\lambda_{L1} \\ \Delta\lambda_{R1} \end{pmatrix} \quad (7)$$

(where $\Delta\lambda$ is expressed in nanometers, $\Delta\varepsilon$ in με (microstrain) and ΔT in °C).

By recording the wavelength response of Left Peak 1, $\Delta\lambda_{L1}$, and Right Peak 1, $\Delta\lambda_{R1}$, the SFS structure can be used simultaneously to measure the axial strain and temperature (within the range used in these tests) of 0-600με and 25.3°C to

58°C. According to Equation (6), (and using an OSA with a wavelength resolution of 15pm), the theoretical strain and temperature resolutions of the proposed sensor are ±4.7με and ±0.2°C, respectively.

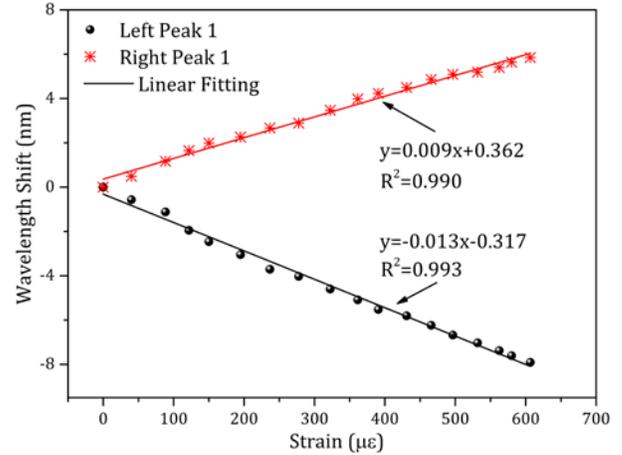

Fig. 5. Wavelength shifts of Left Peak 1 and Right Peak 1 from the sensor system over the strain range from 0 to 600με.
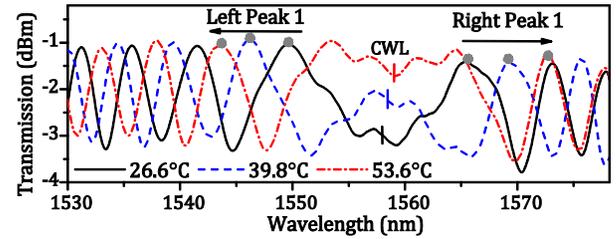

Fig. 6. Transmission spectra of the SFS sensor at temperatures of 26.6°C, 39.8°C and 53.6°C.
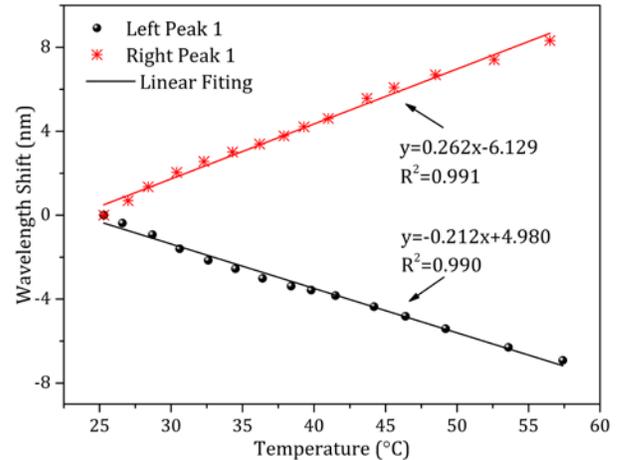

Fig. 7. Wavelength shifts of Left Peak 1 and Right Peak 1, observed over the temperature range from 25.3 to 58°C.

As the strain or temperature applied to the FMF section increases, the CWL, as shown in Fig. 4 and Fig. 6, will also shift with the strain and temperature variations. By calculating the CWL values for the transmission spectra [15], the CWL shifts over the strain range of 0-600με and temperature range of 25.3°C to 58°C are depicted in Fig. 8 and Fig. 9, respectively. As shown in Fig. 8 and Fig. 9, the CWL shifts linearly with a strain sensitivity of -0.001nm/με and a temperature sensitivity

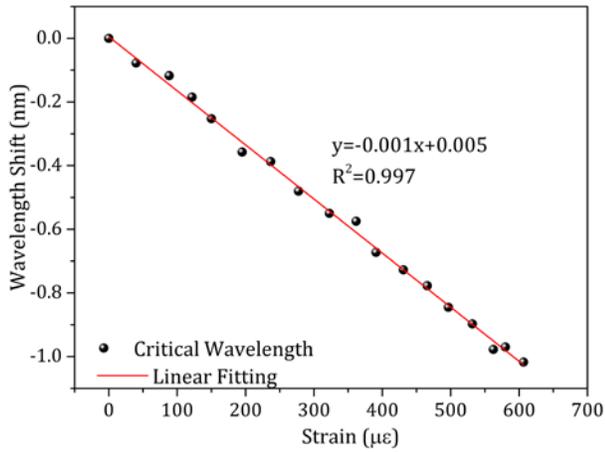of 0.042nm/⁰C, with linear correlation coefficients of 0.997 and 0.986, respectively.

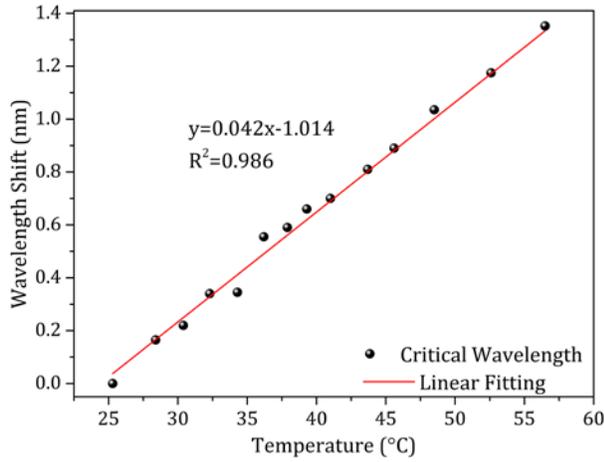Fig. 8. Wavelength shift of CWL over the strain range from 0 to 600με.

Fig. 9. Wavelength shift of CWL over the temperature range from 25.3 to 58⁰C.

Noting the outcomes of previous studies [11-15], compared with the peaks in the transmission spectrum, the CWL shifts monotonically with strain and temperature over this large measurement range. However, because the strain and temperature sensitivities of the CWL are much smaller than those of the Left Peak 1 or Right Peak 1, if the CWL and Left Peak 1 (or Right Peak 1) are combined to demodulate simultaneously the strain and temperature variations, the sensing scheme will lose accuracy because of the larger theoretical strain and temperature resolutions, as shown in Table I.

TABLE I
THEORETICAL RESOLUTIONS OF DIFFERENT WAVELENGTH COMBINATIONS

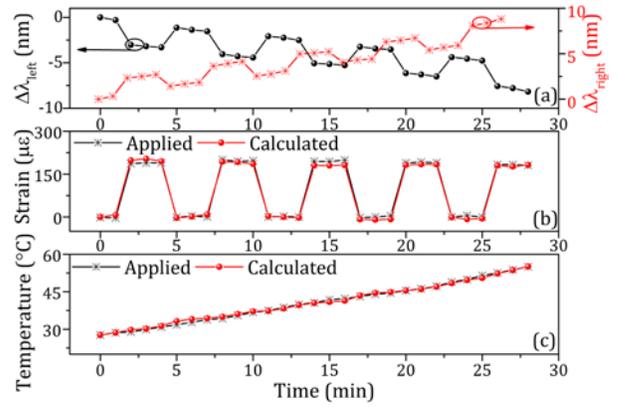| Theoretical Resolutions		
Measured Wavelength	Strain (με)	Temperature (⁰C)
Left Peak 1 and Right Peak 1	±4.7	±0.2
CWL and Left Peak 1	±11.407	±0.629
CWL and Right Peal 1	±44.225	±1.531

Fig. 10. Sensor output for simultaneous change of strain and temperature. (a) shows the values of $\Delta\lambda_{L1}$ and $\Delta\lambda_{R1}$ over the 30-minute period of the experiment; (b) the applied and calculated strains recoded over that time; and (c) the applied and calculated temperatures also recorded over that time.

In order to verify the sensing scheme discussed using Left Peak 1 and Right Peak 1, the outcomes of an actual experiment to allow the simultaneous measurement of strain and temperature are shown in Fig. 10. In the experiment, the temperature of the oven was electrically controlled to gradually increase it from room temperature to about 60⁰C during a period of 30 min while, at the same time, a strain of up to 200με was applied in a step function, as shown in the Fig. 10. The output response of the SFS sensor structure designed, allowing the simultaneous demodulation of strain and temperature was calculated by using equation (7), and the calculated results are plotted with the actual, applied values of strain and temperature respectively, in Fig. 10 (b) and (c). The results obtained are in good agreement, as can be seen and within a reasonable level of experimental error. The small differences between the calculated and actual applied values seem likely to result from the uncertainty in the measurement of the actual values imposed e.g. using the outputs of the digital thermometer in the temperature oven and the wavelengths recorded for the FBG change, using the OSA. Also, a quantitative comparison of the performance between the SFS sensor developed in this study and other reported sensing schemes for simultaneous measurement of strain and temperature is shown in Table II. Apart from the advantages of a simple and co-located sensing structure and ease of identification and detection, this proposed SFS sensor structure has relatively high (and indeed different) sensitivities, and high temperature and strain resolutions compared with other sensors, as illustrated by Table II.

TABLE II
QUANTITATIVE COMPARISON OF PERFORMANCE OF THE REPORTED SCHEMES
FOR SIMULTANEOUS MEASUREMENT OF STRAIN AND TEMPERATURE
(Sensor Type 1: Two individual sensors; Sensor Type 2: One compact fiber interferometer with two outputs; Temperature Sensitivity: TS; Strain Sensitivity: SS; Temperature Resolution: TR; Strain Resolution: SR;)

Sensor Type	Ref.	Sensing Scheme	TS	SS	TR (±°C)	SR (±με)
1	[1]	FBG with different grating periods	6.75 pm/°C; 7.25 pm/°C	0.79 pm/με; 0.795 pm/με	5	100
	[2]	FBG with	10.6	1.05	1.6	8.5

		different fiber structures	pm/°C; 9.2 pm/°C	pm/με; 1.04 pm/με		
	[3]	Emission Lines	8.97 pm/°C; 0.0112 mW/°C	0.824 pm/με; -3.090 301×10^{-5}mW/με	Not given	Not given
	[4]	Single LPG using different stop band peaks	290 pm/°C; 490 pm/°C	0; 0.02 pm/με	0.2	405
		LPG pair	310 pm/°C; 500 pm/°C	0; 0.8 pm/με	0.4	265
	[5]	Fluorescent fiber techniques	1.705-1.92×10^{-3} FPPR/°C; 0.01027 pm/°C	0; 1.15 pm/με	2.5	36
2	[6]	Suspended core photonic crystal fiber	25.30 pm/°C; -6.01 pm/°C	0.34 pm/με; -3.16 pm/με	0.45	4.02
	[7]	Liquid-filled photonic crystal fiber	42.818 nm/°C; -11.343 nm/°C	-38.041 pm/με; 8.702 pm/με	Not given	Not given
	[8]	Fiber taper and lateral-shifted junction	60.4 pm/°C; 63.9 pm/°C	-1.47 pm/με; -2.71 pm/με	Not given	Not given
	This Study	Few mode fiber	-212pm/°C; 262pm/°C	-13 pm/με; 9 pm/με	0.2	4.7

IV. Discussion

A novel fiber in-line MZI sensor system for the simultaneous measurement of strain and temperature has been proposed and demonstrated in this paper, with results obtained lying within the experimental error of the measurement of the parameters recorded, temperature and strain. The sensor head is simple and easy to fabricate – this has been done by splicing a piece of 20cm FMF between two segments of SMF to create the sensor itself. The applied strain and temperature changes were obtained by measuring the wavelength shifts of Left Peak 1 and Right Peak 1 in the transmission spectra of the SFS structure that forms the core of the sensor. This fiber sensor device has the merits of being simple, easy to fabricate and low cost, which makes it useful for a number of practical applications.

The approach discussed in this paper allows a very compact sensor to be created which can be 'packaged' in a number of different ways to fit different circumstances. Further, the 'read-out' from the sensor can be with either an OSA or an FBG interrogator (such as Hyperion si155® from Micron Optics). Thus it can be very competitive with these alternative approaches – for example the suspended core photonic crystal fiber [6], the liquid-filled photonic crystal fiber [7], or the fiber taper and lateral-shifted junction [8] are more complex to

fabricate and devices using fluorescent fiber require the analysis of the decay time or spectral output from the fiber which changes as a function of the measurands. The use of emission line-based methods again will require the use of a suitable spectrometer of appropriate resolution.

The approach discussed in this paper therefore compares very favorably with the alternative methods for the simultaneous measurement of strain and temperature that have been discussed by some of the authors and others as shown in Table II [1 - 8], in terms of the performance achieved, the simplicity of fabrication of the sensor and the ease of use of the device.

References

[1] P. Sivanesan, J. S. Sirkis, Y. Murata, S. G. Buckley, "Optimal wavelength pair selection and accuracy analysis of dual fiber grating sensors for simultaneously measuring strain and temperature", *Opt. Eng.*, vol. 41, pp. 2456-2463, Oct. 2002.
[2] B. O. Guan, H. Y. Tam, S. L. Ho, "Simultaneous strain and temperature measurement using a single fiber Bragg grating", *Electron. Lett.*, vol. 36, pp. 1018-1019, Jun. 2000.
[3] D. Leandro, M. Ams, M. López-Amo, T. Sun, T & K. T. V. Grattan, Simultaneous Measurement of Strain and Temperature Using a Single Emission Line. *J. Lightw. Technol*, 33(12), 2426-2431, 2015
[4] S. K. A. K. Bey, T. Sun, T & K. T. V. Grattan, Simultaneous measurement of temperature and strain with long period grating pairs using low resolution detection. *Sens. Act. A*, 144(1), 83-89, 2008
[5] S. Pal, Y. Shen, J. Mandal, T. Sun, & K. T. V. Grattan, Simultaneous measurement of strain (to 2000 με) and temperature (to 600°C) using a combined Sb-Er-Ge-codoped fiber-fluorescence and grating-based technique. *IEEE Sensors J.*, 5(6), 1462-1467, 2005
[6] S. Rota-Rodrigo, M. López-Amo, J. Kobelke, K. Schuster, J. L. Santos, and O. Frazão, "Multimodal interferometer based on a suspended core fiber for simultaneous measurement of physical parameters", *J. Lightw. Technol.*, vol. 33, no. 12, pp. 2468-2473, Jun. 2015.
[7] H. Liang, W. G. Zhang, P. C. Geng, Y. G. Liu, Z. Wang, J. Q. Guo, S. C. Gao, and S. Y. Yan, "Simultaneous measurement of temperature and force with high sensitivities based on filling different index liquids into photonic crystal fiber", *Opt. Lett.*, vol. 38, no. 7, pp. 1071-1073, Apr. 2013.
[8] P. Lu, Q. Chen, "Asymmetrical fiber Mach–Zehnder interferometer for simultaneous measurement of axial strain and temperature", *IEEE Photon. J.*, vol. 2, no. 6, pp. 942-953, Dec. 2010.
[9] S. M. Tripathi, A. Kumar, E. Marin, and J.-P. Meunier, "Critical wavelength in the transmission spectrum of SMS fiber structure employing GeO2-doped multimode fiber," *IEEE Photon. Technol. Lett.*, vol. 22, no. 11, pp. 799-801, Jun. 1, 2010.
[10] S. Tripathi, A. Kumar, R. K. Varshney, Y. B. P. Kumar, E. Marin,and J.-P. Meunier, "Strain and temperature sensing characteristics of single-mode-multimode-single-mode structures," *J. Lightw. Technol.*, vol. 27, no. 13, pp. 2348-2355, Jul. 1, 2009.
[11] E. Salik, M. Medrano, G. Cohoon, J. Miller, C. Boyter and J. Koh, "SMS fiber sensor utilizing a few-mode fiber exhibits critical wavelength behavior," *IEEE Photon. Technol. Lett.*, vol. 24, no. 7, pp. 593-595, Apr. 1, 2012.
[12] J. Su, X. Dong, and C. Lu, "Characteristics of few mode fiber under bending", *IEEE J. Sel. Top. Quant.*, vol. 22, no. 2, pp. 4402307(1)-4402307(7), Jan. 25, 2016.

[13] J. Su, X. Dong, and C. Lu, "Property of bent few-mode fiber and its application in displacement sensor", *IEEE Photon. Technol. Lett.*, vol. 28, no. 13, pp. 1387-1390, Jul. 1, 2016.

[14] J. Su, X. Dong, and C. Lu, "Intensity detection scheme of sensors based on the modal interference effect of few mode fiber", *Measurement*, vol. 79, pp. 182-187, Feb. 2016.

[15] C. Lu, X. Dong, and J. Su, "Detection of Refractive Index Change From the Critical Wavelength of an Etched Few Mode Fiber", *J. Lightw. Technol.*, vol. 35, no. 13, pp. 2593-2597, Jul. 1. 2017.

[16] Article comprising a dispersion-compensating optical waveguide, by A. M. Vengsarkar, K. L. Walker. (1995, Sep. 5). *U. S. Patent No. 5448674* [Online]. Available: https://search.glgoo.com/patents/US5448674

[17] C. Wei, G. Lin, X. Dong and S. Tao, "A tunable polarization-independent comb filter based on high-order mode fiber", *J. Opt.*, vol. 15, no. 5, pp. 055403(1)-055403(6), Mar. 2013.

[18] C. D. Poole, J. M. Wiesenfeld, D. J. DiGiovanni, and A. M. Vengsarkar, "Optical fiber-based dispersion compensation using higher order modes near cutoff," *J. Lightwave Technol*, vol. 12, no. 10, pp. 1746-1758, Oct. 1994.

[19] M. G. Xu, J.-L. Archambault, L. Reekie, and J. P. Dakin, "Discrimination between strain and temperature effects using dual-wavelength fiber grating sensors", *Electron. Lett.,* vol. 30, no. 13, pp. 1085-1087, Jun. 23, 1994.

[20] W. Jin, W. C. Michie, G. Thursby, M. Konstantaki, and B. Culshaw, "Simultaneous measurement of strain and temperature: Error analysis", *Opt. Eng.*, vol. 36, no. 2, pp. 598-609, Feb. 1997.